## PAPER

Check for updates

# A facile one-pot synthesis of tetrahydrobenzo[b]pyrans and 2-amino-4H-chromenes under green conditions†

Sarieh Momeni and Ramin Ghorbani-Vaghei [ID] *

This research developed a new nanocatalyst by incorporating nanocopper iodide onto the surface of a layered double hydroxides modified. This new nanocatalyst enables the green synthesis of tetrahydrobenzo[b]pyrans and 2-amino-4H-chromene derivatives through a one-pot, three-component reaction, demonstrating remarkable activity and selectivity. Key advantages of this method include increased products yield (86–96%), rapid reaction kinetics (5–23 minutes), low reaction temperature (40 °C), synthesis of new products, straightforward purification methods, catalyst recyclability (up to 4 cycles), and solvent-free conditions.

## 1. Introduction

Layered double hydroxides (LDHs), a widely studied class of inorganic layered materials, exhibit remarkable capability for anion intercalation. They possess two-dimensional nanostructures described by the formula $[M_{(1-x)}^{2+}M_x^{3+}(OH)_2](A^{n-})_{x/n}\cdot zH_2O]$, where $M^{2+}$ and $M^{3+}$ represent divalent and trivalent metal ions, respectively. These metal ions, including $Zn^{2+}$, $Mg^{2+}$, $Ca^{2+}$, $Mn^{2+}$, $Co^{2+}$, $Fe^{2+}$, $Al^{3+}$, $Cr^{3+}$, $Fe^{3+}$, $Co^{3+}$, and $Mn^{3+}$, replace each other interchangeably in the structure. The interlayer anions, often chloride, bromide, carbonate, or nitrate, along with the molar ratio $x$ (ranging from 0.20 to 0.33), play a crucial role in preventing unfavorable phase formation.[1–3] LDHs possessing abundant basic sites within their brucite-like layers serve as effective heterogeneous solid base catalysts, finding extensive applications in organic synthesis, including but not limited to Michael addition, aldol and Claisen–Schmidt condensation, and Knoevenagel condensation. LDH nanostructures show promise across various fields like adsorption, photochemistry, catalysis, molecular recognition, and catalysis.[4–6] Particularly in biomedicine, their layered structure and ability for anionic exchange make them significant. Notably, LDH nanoparticles excel in drug delivery, allowing for encapsulation of specific compounds through interlayer anion exchange.[7]

Nanomaterials have revolutionized catalytic chemistry, offering unprecedented opportunities for enhancing reaction efficiency and selectivity while minimizing environmental impact. These materials, engineered at the nanoscale, possess unique properties such as high surface area-to-volume ratio, tunable surface chemistry, and size-dependent reactivity, making them ideal candidates for catalytic applications.[8,9]

The development of materials through chemical synthesis is evolving with a fresh perspective on environmental stewardship. Researchers in this domain are progressively incorporating eco-conscious techniques, such as employing non-toxic solvents, conducting reactions without solvents, employing recyclable catalysts, and embracing one-pot multicomponent reactions. These methods are aimed at mitigating the environmental effects of chemical processes.[10,11]

Multi-component reactions (MCRs) have emerged and expanded as a potent strategy for synthesizing a broad array of drug-like compounds with diverse structures. Key benefits of this approach include high yields, shortened reaction times, enhanced atomic economy, and reductions in both solvent usage and energy consumption.[12,13]

In recent years, nitrogen-linked heterocyclic compounds have garnered significant interest owing to their extensive utility across various applications.[14,15] Tetrahydrobenzo[b]pyrans, also referred to as tetrahydro-4H-chromenes, are highly esteemed fused oxygen-containing heterocycles appreciated for their diverse applications in synthetic organic and medicinal chemistry.[16–18] They encompass a wide range of biological activities, including anticancer,[19] anti-coagulant,[20] anti-HIV,[21] antibacterial,[22] antiviral,[23] anti-inflammatory,[24] diuretic, antihypertensive,[25] antioxidant.[14] Notably, several of these heterocycles hold promise in the treatment of conditions such as Schizophrenia, Alzheimer's, amyotrophic lateral sclerosis, Huntington's, Parkinson's, and Down's syndrome. These reactions employ a variety of catalytic systems, such as $CeCl_3\cdot 7H_2O$,[26] $Fe_3O_4@SiO_2@NiSB$,[27] $[DABCO-PDO][CH_3COO]$,[28] $Co_3(PO_4)_2$,[29] $NH_2@SiO_2@Fe_3O_4$ MNPs,[30] f rGO@Fe_3O_4@ZrCp_2Cl_2 ionic liquid [PEMIM][OH],[31] and Nano-SiO_2/DBN.[32] Moreover, alternative synthesis conditions like electrochemical conditions and microwave radiation have also been documented.

The chromene ring system has garnered significant interest in pharmaceutical research due to the diverse biological properties observed in synthetic and natural chromene derivatives,

Department of Organic Chemistry, Faculty of Chemistry and Petroleum Sciences, Bu-Ali Sina University, Hamedan, Iran. E-mail: rgvaghei@yahoo.com; ghorbani@basu.ac.ir

† Electronic supplementary information (ESI) available. See DOI: https://doi.org/10.1039/d4ra04239e

**Paper**

such as antibacterial,[33] antimicrobial,[34] anti-inflammatory,[35] antiproliferative, antifungal,[36] and anticancer activities.[37] Notably, the synthesis of 2-amino-4H-chromenes and their derivatives *via* multi-component reactions (MCRs) involving aromatic aldehydes, resorcinol, and malononitrile has been explored. Various catalyst systems have been employed for this synthesis, such as tungstic acid-SBA-15,[38] Fe$_3$O$_4$-chitosan nanoparticles,[39] CuO–CeO$_2$,[40] nano-sized MgO,[41] sulfonic acid-functionalized MIL-101(Cr),[42] potassium phthalimide-N-oxyl (POPINO),[43] K$_2$CO$_3$,[44] Na$_2$CO$_3$,[45] and Mg/Al-HT.[46]

Yet, given the sustained interest in this domain, there remains a call for research into uncomplicated methodologies, reduced reaction times, and catalysts that are both more efficient and reusable, to meet the ongoing demand for the synthesis of 2-amino-4H-chromenes and tetrahydrobenzo[b] pyrans derivatives in one-pot reactions.

Continuing our pursuit of advancing eco-friendly heterogeneous nanocatalysts and their utilization in catalyzing organic reactions and synthesizing heterocyclic compounds, we present the synthesis and characterization of CuI stabilized on LDH functionalized with a sulfonamide ligand. LDH@PTRMS@NDBD@CuI served as a highly effective and reusable heterogeneous nanocatalyst in facilitating the three-component one-pot synthesis of 4H-chromene (**4a–h**) and tetrahydrochromene.

# 2. Experimental

## 2.1. General

In this study, chemicals were obtained from Merck and used without additional purification. Characterization methods included FT-IR spectroscopy with a PerkinElmer GX FT-IR spectrometer, 1H and $^{13}$C NMR spectroscopy in DMSO-d$_6$ using Bruker BioSpin GmbH 300 MHz FT NMR spectrometers, and melting point determination using a BUCHI 510 device. The novel LDH@PTRMS@NDBD@CuI catalyst was thoroughly characterized through FTIR, EDX, mapping, XRD, FESEM, TGA, and DSC analyses. XRD patterns were taken with a Philips PW1730 in the range of 10 to 90° (2$\theta$), and FESEM analysis was performed using a FE-SEM TESCAN MIRA3 instrument. EDX analysis was conducted with EDAX-EDS equipment, TGA was performed using a TGA-DTA instrument in a nitrogen atmosphere, and DSC measurements were taken with a DSC device. The progress of reactions and material purity were monitored using thin layer chromatography (TLC) and silica gel plates.

## 2.2. Protocol for synthesizing layered double hydroxides (Zn/Cr-LDHs)

The synthesis of Zn/Cr-LDH followed the previously described procedure, outlined as follows: initially, Zn(NO$_3$)$_2$·6H$_2$O and Cr(NO$_3$)$_3$·9H$_2$O salts were dissolved in deionized water in a 2:1
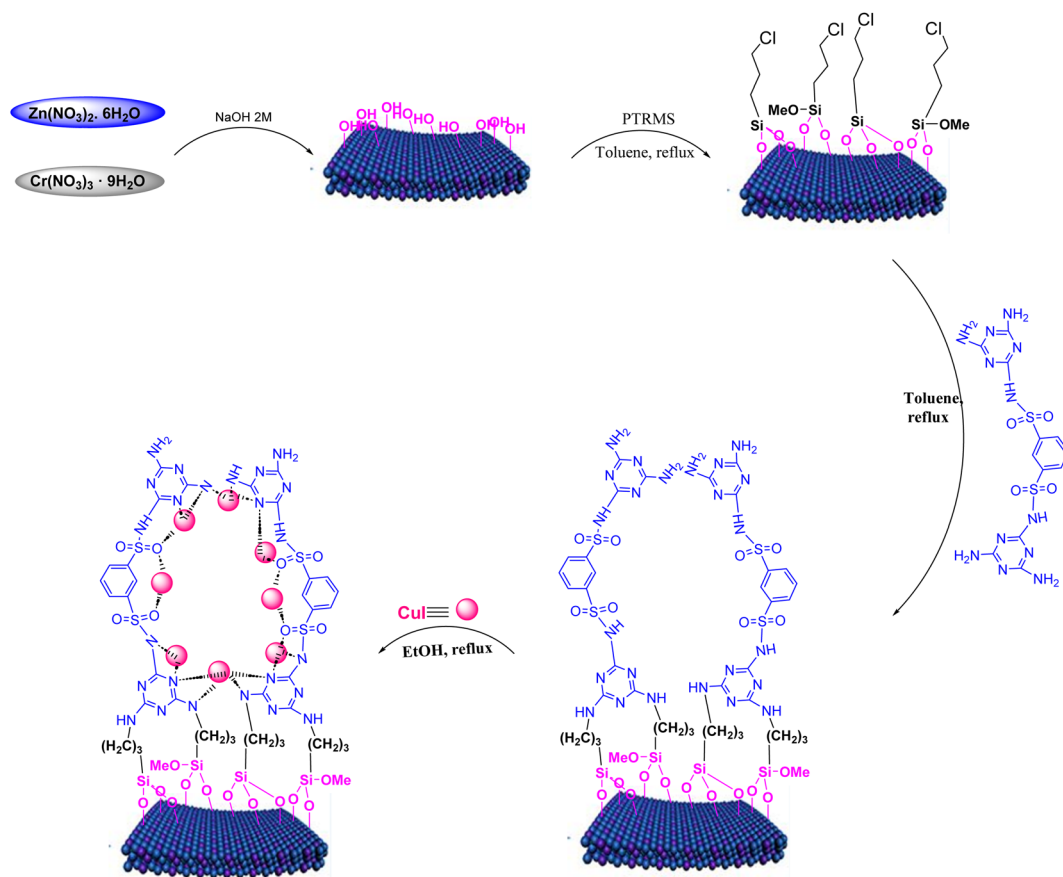


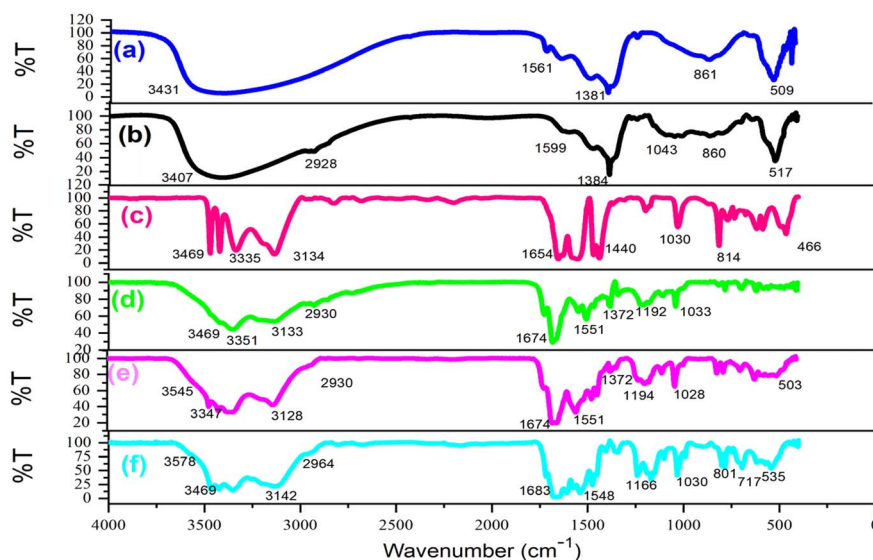Scheme 1 The steps of catalytic LDH@PTRMS@NDBD@CuI synthesis.

**Fig. 1** FTIR spectra of (a) double hydroxide layer, (b) LDH@PTRMS, (c) melamine (d) NDBD ligand, (e) LDH@PTRMS@NDBD and (f) LDH@PTRMS@NDBD@CuI.

molar ratio. The solution's pH was subsequently raised to 11.5 by titrating with a 2 M NaOH aqueous solution while vigorously stirring, and this pH level was upheld for a duration of 18 hours at constant temperature. After filtration, the resulting turquoise product incurred washing with distilled water, followed by drying in an oven at 50 °C for 24 hours.[6]

### 2.3. Method for synthesizing LDHs coated with 3-chloropropyltrimethoxysilane (Zn/Cr-LDH@PTRMS)

To activate LDH, we employed 3-chloropropyltrimethoxysilane (PTRMS). Initially, 1 g of pre-synthesized LDH was dispersed within a 100 mL balloon containing 50 mL of toluene. Next, 2 mL of PTRMS was introduced into the solution, which was refluxed for 24 h with continuous stirring. Following refluxing, a precipitate formed, which was collected using filter paper. Subsequently, the precipitate incurred multiple washes with toluene and ethanol to eliminate impurities. Finally, the washed material was dried in an oven at 50 °C to ensure the complete removal of solvents and moisture.[6]

### 2.4. Method for synthesizing ligand of $N_1,N_4$-bis(4,6-diamino-1,3,5-triazin-2-yl)benzene-1,4-disulfonamide (NDBD)

To begin, phosphorus pentachloride, acting as the chlorinating reagent, was introduced, totaling 16.5 mmol, into a vessel containing 5.00 g (18 mmol) of 1,3-benzenedisulfonic acid disodium salt. The mixture was then heated to 65 °C, allowing the reaction to proceed for 2 hours. Following completion, a solution composed of 150 g of dry ice and 150 mL of chloroform was added, facilitating the separation of the organic layer containing 1,3-benzenedisulfonyl chloride.

Following the separation, 1,3-benzenedisulfonyl chloride (2 mmol) was dissolved in 30 mL of toluene solvent in a 50 mL round-bottom flask. Concurrently, melamine (4 mmol) was dissolved in toluene within a distinct vessel, and this melamine–toluene solution was carefully introduced drop by drop into the

flask. Subsequently, the flask was refluxed for a duration of 24 hours. Following this, the resultant precipitate was filtered and subjected to multiple washes with acetonitrile (3 mL each). Finally, the product was dried at 60 °C for a period of 18 hours.[2]

### 2.5. Method for synthesizing LDH@PTRMS@NDBD

LDH@TRMS (0.3 g) was introduced into a 250 mL round-bottom flask containing toluene (80 mL) as the solvent. The mixture incurred ultrasonication for 30 minutes. Next, the ligand NDBD (0.55 g) was incorporated, and the solution was stirred under reflux conditions for 48 hours. Afterward, the resulting mixture was filtered and subjected to several washes with toluene (2 mL) and one wash with ethanol (2 mL). Lastly, the product was dried in an oven at 60 °C for 24 hours.[2]

### 2.6. Method for synthesizing copper iodide (CuI) nanoparticles

CuSO$_4$ (1 mmol) was ultrasonically treated in acetone, followed by a HCl (2 M) solution, and then rinsed several times with distilled water. After drying, the copper sulfate was added to
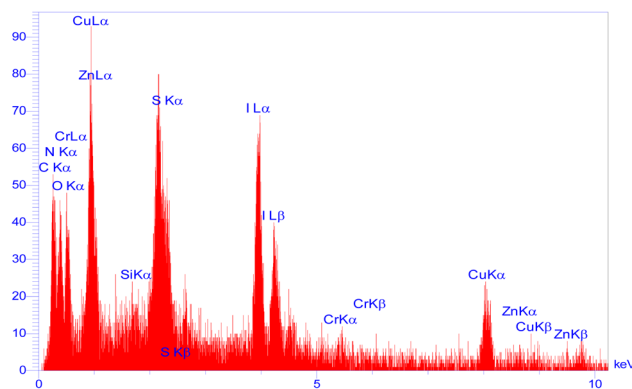


**Fig. 2** EDX analysis of LDH@PTRMS@NDBD@CuI catalyst.

a solution of KI (2 mmol) in 40 mL of distilled water and subjected to ultrasound for 30 minutes. The resulting purple precipitate was separated by centrifugation, washed with distilled water and ethanol, and then dried in an oven at 60 °C for 24 hours.

### 2.7. Method for synthesizing LDH@PTRMS@NDBD@CuI

In a 25 mL flask, 0.3 g of copper iodide nanoparticles were combined with 0.5 g of LDH@TRMS@NDBD powder, and dissolved in 20 mL of ethanol. The resulting reaction mixture was reflux for 24 hours while being stirred with a magnetic stirrer. Subsequently, LDH@PTRMS@NDBD@CuI nanoparticles were obtained through centrifugation, followed by three washes with ethanol (4 mL each). Finally, the nanoparticles were dried in an oven at 60 °C, the steps of catalytic LDH@PTRMS@NDBD@CuI synthesis were illustrated in Scheme 1.

### 2.8. Method for synthesizing tetrahydrobenzo[*b*]pyrans and 2-amino-4*H*-chromenes derivatives in the presence of LDH@PTRMS@NDBD@CuI nanoparticles

Malononitrile (1 mmol), along with dimedone or resorcinol (1 mmol) and various derivatives of aromatic aldehydes (1 mmol), were combined with LDH@PTRMS@NDBD@CuI nanoparticles (0.05 g) under solvent-free conditions at 40 °C. The mixture was blended in a test tube and stirred for an appropriate duration (5 to 23 minutes) using a magnetic stirrer. The progression of the reaction was monitored using TLC (ethyl acetate/normal hexane: 4/8). Once the reaction reached its conclusion and the desired compound was formed, the mixture was cooled until it reached the room temperature. To separate the catalyst, 3 mL of hot ethanol or ethyl acetate was added to the mixture, followed by stirring for 2 minutes. Following that, the catalyst (LDH@PTRMS@NDBD@CuI)
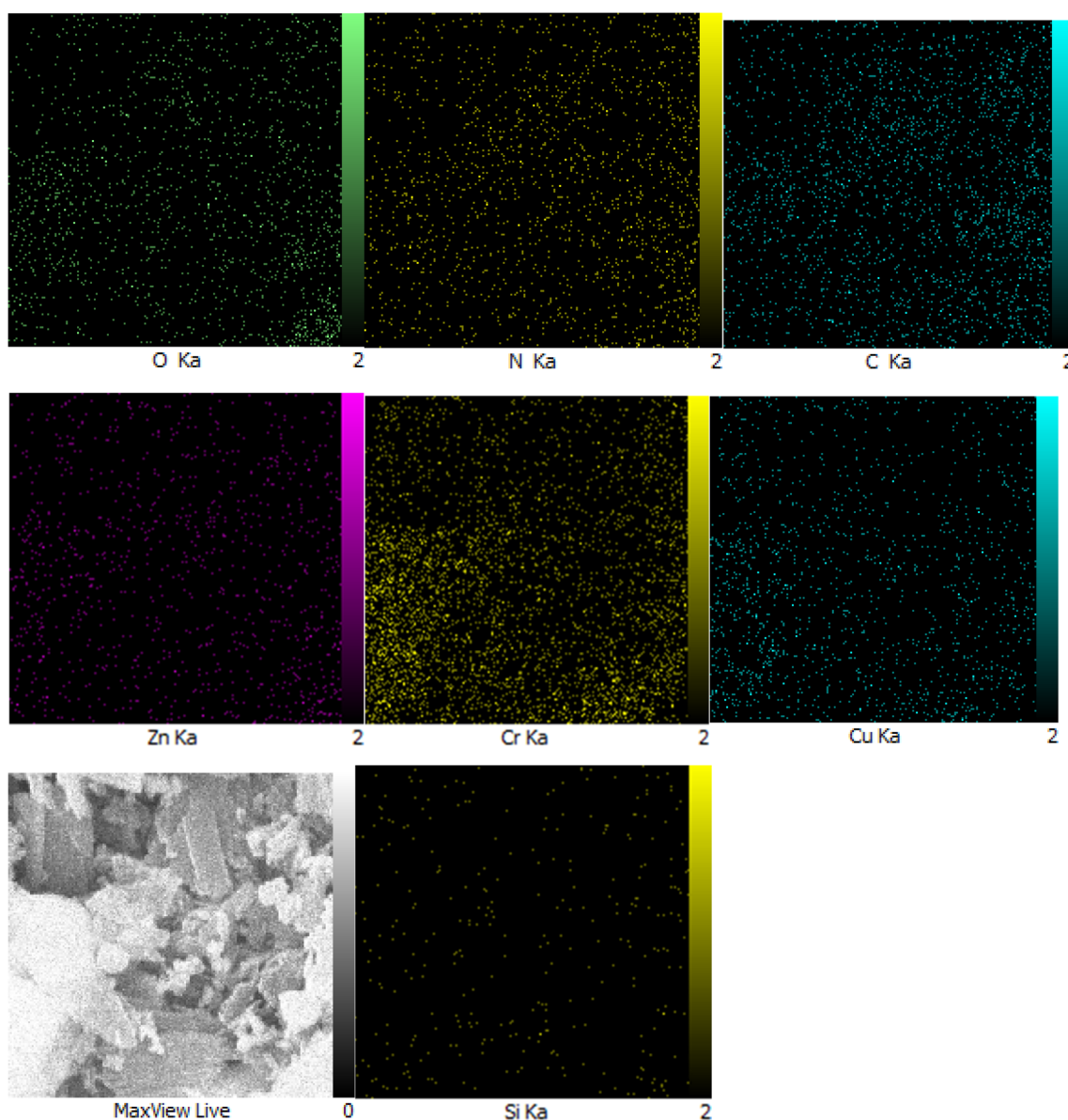


**Fig. 3** Elemental mapping analysis (MAPPING) of LDH@PTRMS@NDBD@CuI catalyst.

was separated through centrifugation, subjected to washing, and subsequently dried in an oven set at 60 °C.

The solvent within the reaction mixture was evaporated, and the resultant products were dissolved in ethanol using nebulization. The synthesis of the compounds was accomplished with remarkable efficiency, as illustrated in Table 5.

FTIR, $^1$H NMR, and $^{13}$C NMR spectra were utilized to identify the products, with the melting points of all products being determined.

# 3. Results and discussions

### 3.1. Spectroscopic investigation to identify nanocopper catalyst stabilized on double hydroxide layer coated with ligand of NDBD

Following the synthesis of the catalyst, a comprehensive array of analyses such as Fourier-transform infrared spectroscopy (FT-IR), field emission scanning electron microscopy (FESEM), X-ray dispersive analysis (EDX), elemental imaging, X-ray diffraction (XRD), and thermal decomposition (DSC, TGA) were conducted to confirm and characterize the LDH@PTRMS@NDBD@Cu catalyst. Fig. 1 illustrates the FT-IR spectrum of (a) the double hydroxide layer, (b) LDH@PTRMS, (c) melamine, (d) the ligand (NDBD), (e) LDH@PTRMS@NDBD, and a portion of LDH@PTRMS@NDBD@CuI is represented by (f).

Section (a) depicts LDH, characterized by peaks ranging from 2500 to 3490 cm$^{-1}$ attributed to the hydroxides present on LDH, while those within the range of 1380–1400 cm$^{-1}$ signify the stretching vibrations of the interlayer nitrate anion. Furthermore, the peak observed at 853 cm$^{-1}$ corresponds to metal–oxygen stretching vibrations.[47] In contrast, section (b) illustrates LDH functionalized with 3-chloropropyltrimethoxysilane, as
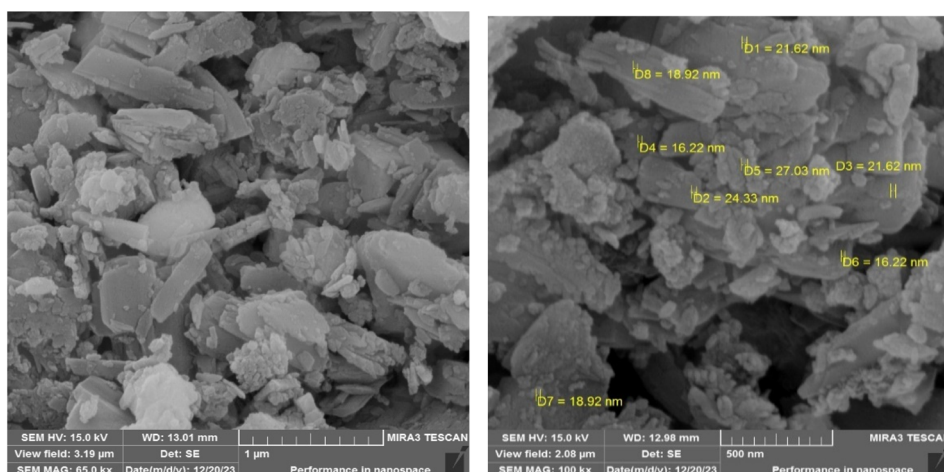


Fig. 4   FESEM images of Zn/Cr-LDH@PTRMS@NDBD@CuI catalyst.
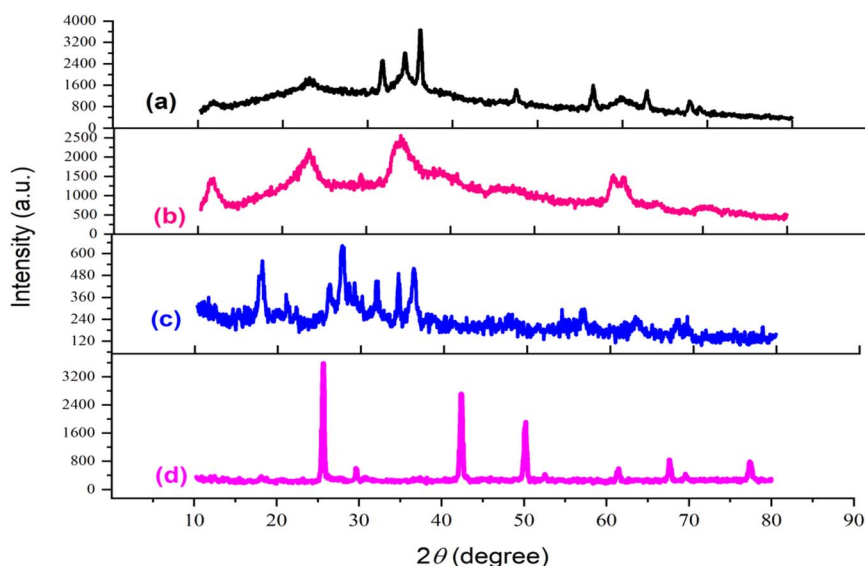


Fig. 5   X-ray diffraction of the catalyst and its intermediates (a) double hydroxide layer, (b) LDH@PTRMS, (c) LDH@PTRMS@NDBD and (d) LDH@PTRMS@NDBD@CuI.
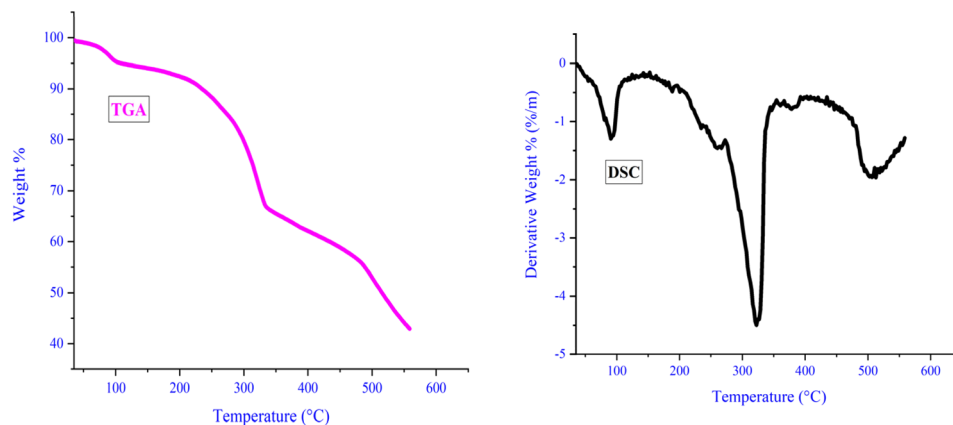
**Fig. 6** TGA and DSC thermal analyzes of Zn/Cr-LDH@PTRMS@NDBD@CuI catalyst.

indicated by the peak at 2800 cm$^{-1}$, which signifies C–H stretching vibrations.[47]

In segment (c) of the spectrum, which corresponds to melamine, peaks associated with NH are evident within the range of 3133–3470 cm$^{-1}$, while stretching vibrations of the ring cyanide are apparent at 1652 cm$^{-1}$ and 1631 cm$^{-1}$.[2] Moving to segment (d) attributed to the NDBD ligand, peaks within the

3180–3410 cm$^{-1}$ range correspond to NH stretching vibrations.[2] Additionally, the peak at 1722 cm$^{-1}$, previously associated with ring cyanide stretching vibrations at 1652 cm$^{-1}$, has shifted due to the formation of the amide group near the ring C=N. Another peak at 1679 cm$^{-1}$, originally from the region 1631 cm$^{-1}$, is also linked to ring cyanide vibrations. Moreover, the peaks observed at 1361 and 1144 cm$^{-1}$ are attributable to

**Table 1** Optimization of reaction conditions for the synthesis of 2-amino-4-(4-chlorophenyl)-7,7-dimethyl-5-oxo-5,6,7,8-tetrahydro-4*H*-chromen-3-carbonitrile derivative
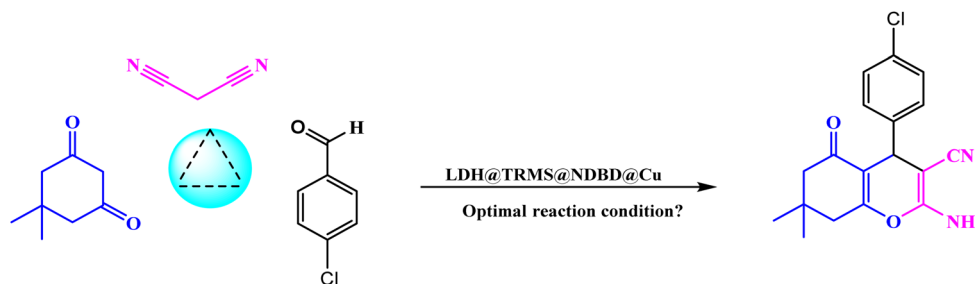


| Entry | Solvent | Load of catalyst (mg) | Temperature (°C) | Time (min) | Yield (%) |
|---|---|---|---|---|---|
| 1 | — | — | 70 | 60 | 28 |
| 2 | — | 10 | r.t | 15 | 70 |
| 3 | — | 10 | 40 | 13 | 73 |
| 4 | — | 20 | r.t | 12 | 81 |
| 5 | — | 20 | 40 | 10 | 84 |
| 6 | — | 35 | r.t | 11 | 87 |
| 7 | — | 40 | 40 | 12 | 89 |
| 8 | — | 45 | 50 | 7 | 94 |
| 9 | — | 50 | r.t | 6 | 92 |
| 10 | — | 55 | 40 | 6 | 96 |
| 11 | — | 50 | 40 | 5 | 96 |
| 12 | — | 50 | 60 | 5 | 96 |
| 13 | — | 50 | 80 | 3 | 96 |
| 14 | EtOH | 45 | 40 | 7 | 92 |
| 15 | MeOH | 45 | 40 | 9 | 45 |
| 16 | H$_2$O | 45 | 40 | 10 | 75 |
| 17 | EtOAc | 45 | 40 | 13 | 88 |
| 18 | *n*-Hexane | 45 | 40 | 20 | 72 |

**Table 2** Comparison of the catalytic activity of Zn/Cr-LDH@PTRMS@NDBD@CuI and its related intermediates by performing the model reaction[a]

| Entry | Catalyst | Time | Yield[b] (%) |
|---|---|---|---|
| 1 | LDH | 20 | 38 |
| 2 | LDH@TRMS | 20 | 40 |
| 3 | LDH@TRMS@NDBD | 20 | 58 |
| 4 | LDH@TRMS@NDBD@CuI | 5 | 96 |

[a] Reaction condition: malononitrile (1 mmol), dimedone (1 mmol) and 4-chlorobenzaldehyde (1 mmol). [b] Isolated yields.

**Table 4** Comparison of the catalytic activity of Zn/Cr-LDH@PTRMS@NDBD@CuI and its related intermediates by performing the model reaction[a]

| Entry | Catalyst | Time | Yield[b] (%) |
|---|---|---|---|
| 1 | LDH | 20 | 25 |
| 2 | LDH@TRMS | 20 | 38 |
| 3 | LDH@TRMS@NDBD | 20 | 56 |
| 4 | LDH@TRMS@NDBD@CuI | 10 | 94 |

[a] Reaction condition: malononitrile (1 mmol), resorcinol (1 mmol) and 4-chlorobenzaldehyde (1 mmol). [b] Isolated yields.

the stretching vibrations of SO. In segment (e), where the O–H peaks are concealed and the ligand is introduced, vibrations associated with NH (3110–3410 cm$^{-1}$) and SO (1357 and 1141 cm$^{-1}$) are detected. Furthermore, the appearance of the peak at 2956 cm$^{-1}$ aligns with the CH stretching vibrations of the PTRMS, validating the complete bonding of the ligand to LDH.[2]

In the final step (f), notable reductions in the stretching vibrations of NH and sulfonyl amide groups are observed, while peaks at 517, 574, and 1384 cm$^{-1}$ are indicative of copper iodide presence, confirming its successful immobilization onto the catalyst.

Moreover, another investigation involved elemental determination analysis utilizing energy dispersive spectrometer to examine the constituent elements comprising Zn/Cr-LDH@PTRMS@NDBD@CuI nanocatalyst. The outcomes of this examination validated the existence of N, C, S, O, Si, Cu, Zn, and Cr elements within the catalyst's structure (refer to Fig. 2). Furthermore, as depicted in Fig. 3, the elemental analysis of the composition reaffirms the presence of all aforementioned elements.

To explore the structure, morphology, and particle dimensions of the LDH@TRMS@NDBD@CuI nanocatalyst, images obtained from FESEM analysis are presented in Fig. 4. The

**Table 3** Refining the reaction conditions for synthesizing the derivative 2-amino-4-(4-chlorophenyl)-7-hydroxy-4H-chromene-3-carbonitrile
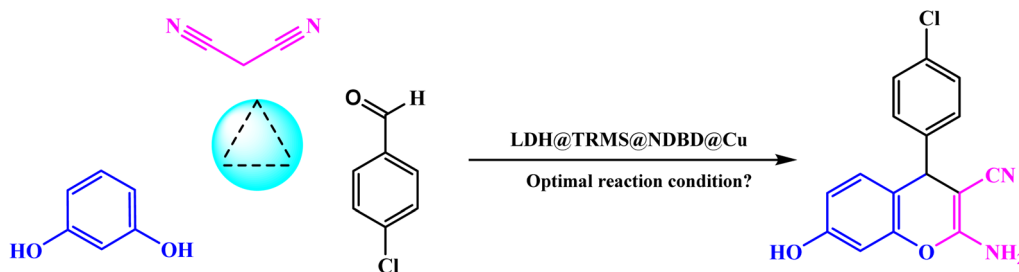


| Entry | Solvent | Load of catalyst (mg) | Temperature (°C) | Time (min) | Yield (%) |
|---|---|---|---|---|---|
| 1 | — | — | 70 | 60 | 22 |
| 2 | — | 10 | r.t | 60 | 68 |
| 3 | — | 10 | 40 | 45 | 71 |
| 4 | — | 20 | r.t | 37 | 82 |
| 5 | — | 20 | 40 | 30 | 84 |
| 6 | — | 35 | r.t | 30 | 85 |
| 7 | — | 40 | 40 | 17 | 89 |
| 8 | — | 45 | 50 | 15 | 91 |
| 9 | — | 50 | r.t | 16 | 92 |
| 10 | — | 55 | 40 | 10 | 94 |
| 11 | — | 50 | 40 | 10 | 94 |
| 12 | — | 50 | 60 | 9 | 94 |
| 13 | — | 50 | 80 | 8 | 96 |
| 14 | EtOH | 45 | 40 | 7 | 80 |
| 15 | MeOH | 45 | 40 | 9 | 45 |
| 16 | H$_2$O | 45 | 40 | 10 | Trace |
| 17 | EtOAc | 45 | 40 | 13 | 50 |
| 18 | CH$_3$CN | 45 | 40 | 20 | Trace |

© 2024 The Author(s). Published by the Royal Society of Chemistry

**Paper**

**Table 5** Synthesis of tetrahydrobenzo[*b*]pyrans and 2-amino-4*H*-chromenes derivatives in the vicinity of Zn/Cr-LDH@PTRMS@NDBD@CuI catalyst [40,46,50–53]



*Time in min*, **Yield in %**, M.p (°C)/ M.p (°C)[Lit.] references



4a, 11 min, 90%
228-230/ 227-229 [50]

4b, 5 min, 96%
208-209/207-209 [50]

4c, 9 min, 91%
120-122/186-188 [51]

4d, 6 min, 96%
176-178/ 178-179 [50]

4e, 7 min, 93%
198-200/ 201-203 [52]

4f, 10 min, 91%
201-203/ 196-198 [50]

4g, 12 min, 90%
206-208/–

4h, 15 min, 90%
270-272/ 272-274 [50]

5a, 18 min, 89%
120-122/ new

5b, 20 min, 87%
189-191/ new

5c, 17 min, 88%
145-150/ new

5d, 23 min, 86%
125-127/ new

6a, 16 min, 91%
230-232/ 232-235 [40]

6b, 10 min, 94%
227-229/ 228-230 [53]

6c, 13 min, 94%
254-256/ 257-259 [40]

6d, 10 min, 92%
210-212/ 210-212 [46]

6e, 12 min, 93%
186-188/ 188-190 [46]

6f, 16 min, 88%
108-110/ 111-113 [40]

6g, 11 min, 92%
239-241/ 240-241 [53]

image distinctly reveals the hexagonal and planar layer structure of LDH, measuring approximately 6 μm in size, indicating the preservation of its fundamental structure. Furthermore, the presence of the ligand and CuI metal results in surface roughening of the catalyst, with nanoparticles displaying a consistent and spherical shape. Notably, the nanoparticle size falls within the range of 18 to 28 nm.

X-ray diffraction (XRD) analysis spanning the $2\theta$ region from 10 to 80° was conducted to characterize the catalyst synthesis stages. The patterns corresponding to (a) LDH, (b) LDH@PTRMS, (c) LDH@PTRMS@NDBD, and (d) LDH@PTRMS@NDBD@CuI are depicted in Fig. 5. In part (a), the peaks at 11°, 24°, 34°, 35°, 37°, 48°, 58°, 60°, and 68° correspond respectively to the crystal planes (003), (006), (101), (012), (015), (018), (108), (110), and (113), matching the zinc/chrome-LDH structure.[48] In part (b), related to the activation of the LDH surface with 3-chlorotrimethoxysilane, all the peaks from the previous step are observed with different intensities. Part (c) involves the placement of the ligand on the surface of the activated LDH, leading to changes in the intensity and value of the peaks from the previous step, attributed to the strong interaction with the NDBD ligand. Notably, in part (d), the peaks observed at 10°, 20°, 25°, 40°, 50°, 60°, 70°, and 98° correspond to copper,[49] confirming the successful incorporation of copper iodide metal onto the catalyst. Estimation of the particle size using Scherer's equation reveals an approximate size of 18 nm.

In order to evaluate the catalyst's thermal stability, thermal gravimetric analysis (TGA) was carried out. As illustrated in Fig. 6, the initial weight loss, occurring around 100 °C, likely stems from the evaporation of water and solvents utilized during catalyst synthesis. Subsequent weight loss, observed between 332 and 480 °C, can be attributed to the degradation and dissociation of the ligand bound to LDH. Above 525 °C, further weight loss indicates metal removal and catalyst decomposition. Notably, all discontinuities observed in TGA analysis align with variations noted in differential scanning calorimetry (DSC) analysis. DSC analysis corroborates TGA findings and underscores the catalyst's stability up to 330 °C. The catalyst's ability to withstand such elevated temperatures is credited to the robust interaction between the ligand and LDH, further strengthened by its complexation with copper iodide. This robust interaction serves as an effective safeguard against catalyst decomposition even at lower temperatures.

## 3.2. Catalytic application of LDH@TRMS@NDBD@CuI in the preparation of tetrahydrobenzo[*b*]pyrans and 2-amino-4*H*-chromenes derivatives

Upon confirming the synthesis of the LDH@PTRMS@NDBD@CuI catalyst through the aforementioned analyses, its efficacy in catalyzing the synthesis of tetrahydrobenzo[*b*]pyrans and 2-amino-4*H*-chromenes was investigated *via* a one-pot three-component reaction. To achieve this, a model reaction involving 4-chlorobenzaldehyde (1 mmol), malononitrile (1 mmol), and dimedone (1 mmol) was employed.

In order to fine-tune the reaction parameters and assess catalyst efficiency, various parameters including temperature,
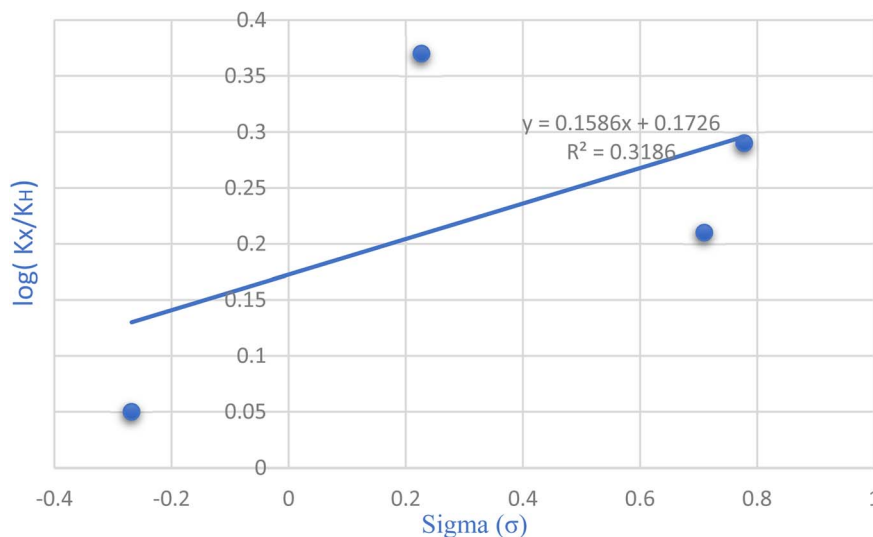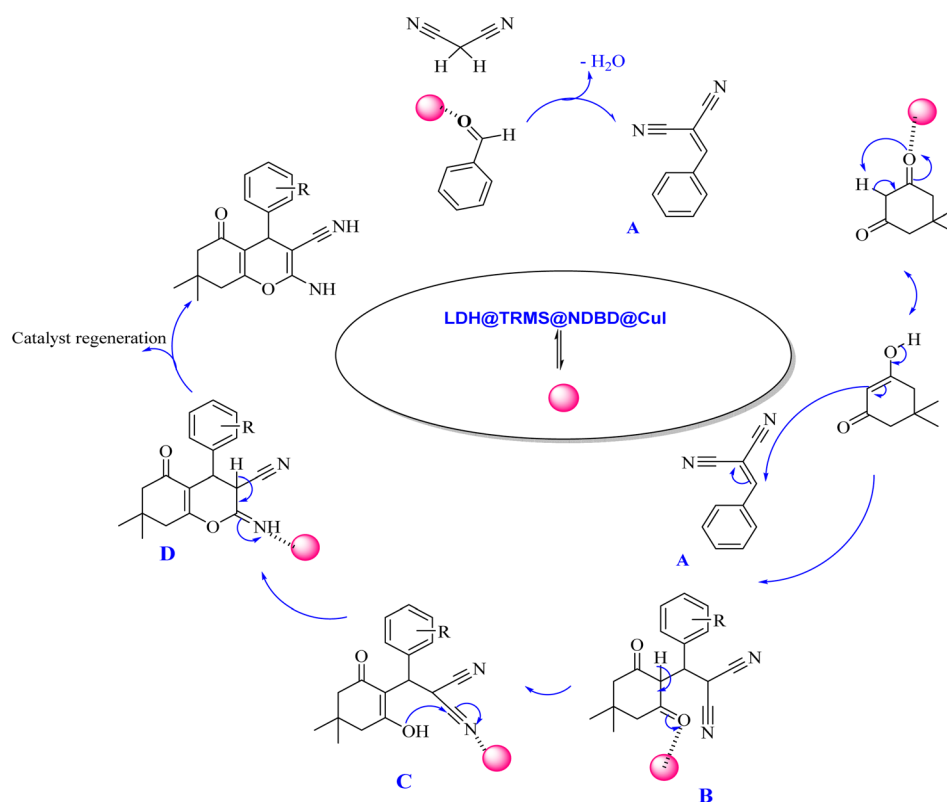
**Fig. 7** Exploring substitution groups in the synthesis of tetrahydrobenzo[*b*]pyrans *via* the Hammett plot.
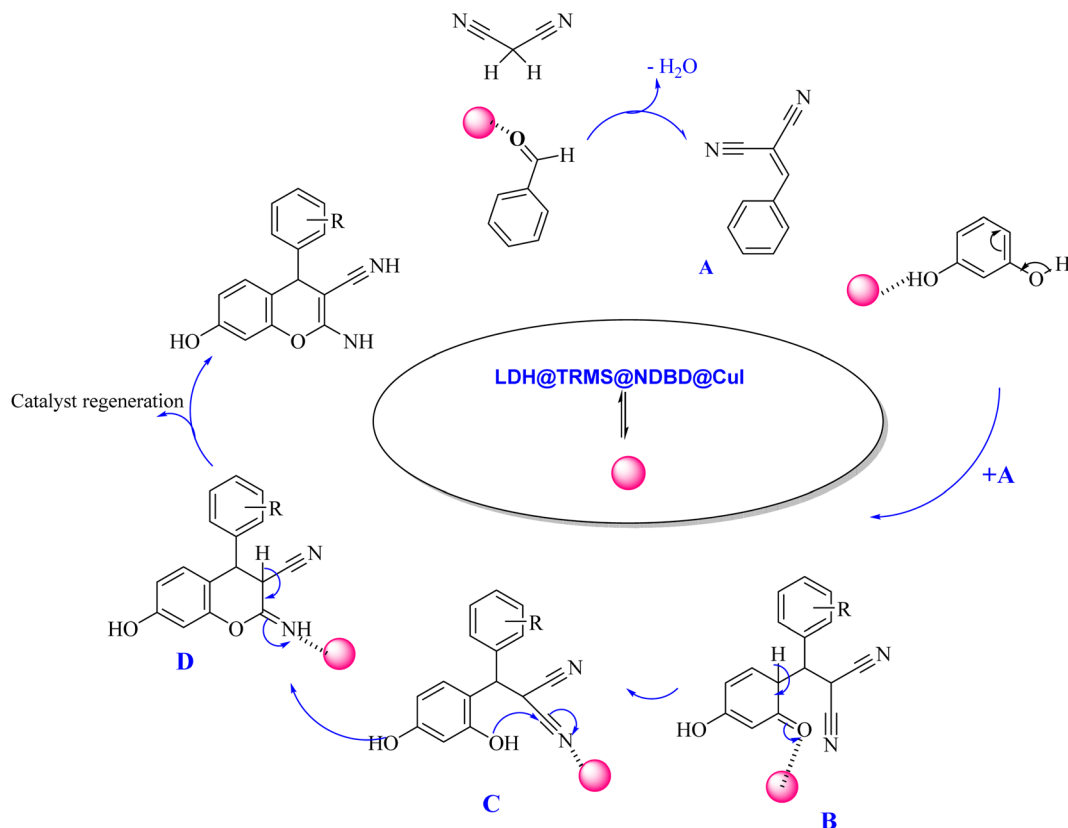


**Scheme 2** Proposed mechanism for the synthesis of tetrahydrobenzo[*b*]pyran derivatives in the vicinity of Zn/Cr-LDH@PTRMS@NDBD@CuI catalyst.

catalyst quantity, solvent choice, and reaction duration were meticulously examined. Additionally, a trial run was performed without the catalyst, yielding a small output. Optimal conditions were determined to be at room temperature with 0.05 g of catalyst. Notably, the protocol's eco-friendly was demonstrated through solvent-free and room temperature reactions. The effective interaction between copper within the catalyst and the

raw materials facilitated high product yields within short timeframes and without solvent usage. Decreased efficiency was observed with lower catalyst quantities, underscoring the catalyst's high effectiveness.

As indicated in Table 1, the model reaction was conducted utilizing ethanol, methanol, ethyl acetate, water, and normal hexane, resulting in a favorable yield. Notably, ethanol solvent

Scheme 3   Proposed mechanism of synthesis of 2-amino-4*H*-chromenes derivatives in the vicinity of Zn/Cr-LDH@PTRMS@NDBD@CuI catalyst.
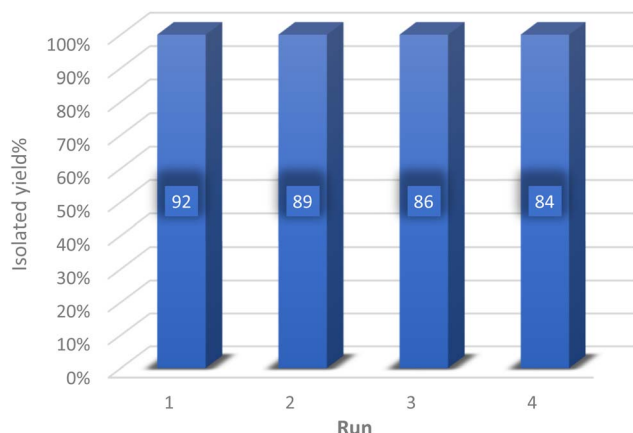


Fig. 8   Ability to recycle and reuse Zn/Cr-LDH@PTRMS@NDBD@CuI catalyst.

exhibited superior yield compared to others. However, the highest efficiency was observed in solvent-free conditions, although the reaction yielded negligible results in the absence of catalyst. Furthermore, the model reaction was investigated with the inclusion of catalytic intermediates, with a summary provided in Table 2. Analysis of the table revealed that LDH, when combined with 3-chlorotrimethoxysilane on its surface, yielded 38% product within half an hour. While LDH alone exhibited consistent product yield, the introduction of the ligand onto the LDH@TRMS surface increased yield to 58%. Remarkably, the highest yield of 96% was achieved within 5

minutes with copper iodide immobilized on the LDH@TRMS@NDBD surface.

Table 3 details the optimization conditions for the model reaction involving 4-chlorobenzaldehyde (1 mmol), malononitrile (1 mmol), and resorcinol (1 mmol), akin to Table 1. This investigation aimed to establish optimal conditions by varying catalyst amounts, temperatures, solvents, and even conducting reactions without solvent, as outlined in Table 3. The most favorable conditions were achieved at a temperature of 40 °C, without solvent, and within a reaction duration of 10 minutes, resulting in an efficiency of 94%.

On the other hand, Table 4 presents the model reaction involving 4-chlorobenzaldehyde, malononitrile, and resorcinol in the presence of catalyst intermediates. Notably, when LDH was utilized, 25% product was obtained in 20 minutes. Incorporating 3-chlorotrimethoxysilane onto the LDH surface increased product yield to 38%, whereas introduction of the ligand onto the LDH@TRMS surface further elevated yield to 56%. Remarkably, the highest product yield of 94% was achieved within 10 minutes with copper iodide immobilized on the LDH surface. TRMS@NDBD configuration exhibited this optimal performance.

To evaluate the efficacy of the novel LDH@PTRMS@NDBD@CuI catalyst, the synthesis of tetrahydrobenzo[*b*]pyrans and 2-amino-4*H*-chromenes derivatives was conducted under optimal conditions. Utilizing malononitrile, dimedone or resorcinol, and a diverse array of benzaldehydes

**Table 6** Assessing the effectiveness of the Zn/Cr-LDH@PTRMS@NDBD@CuI catalyst in producing tetrahydrobenzo[*b*]pyran derivatives relative to other catalystsis

| Entry | Reaction conditions | Time (min) | Yield (%) | Lit. |
|---|---|---|---|---|
| 1 | MCM-41@Schiff base-Co(OAc)$_2$, H$_2$O, 50 °C | 180 | 94 | 54 |
| 2 | rGO@Fe$_3$O$_4$-ZrCp$_2$Cl$_2$, PEG-400, 100 °C | 120 | 80 | 55 |
| 3 | Fe$_3$O$_4$@GO-*N*-(pyridin-4-amine), H$_2$O, reflux | 30 | 92 | 56 |
| 4 | NH$_4$Al(SO$_4$)$_2$·12H$_2$O (Alum)/EtOH/80 °C | 130 | 90 | 57 |
| 5 | NiFe$_2$O$_4$@SiO$_2$-H$_3$PW$_{12}$O$_{40}$, EtOH, reflux | 15 | 89 | 58 |
| 6 | PPI/H$_2$O/reflux | 15 | 90 | 59 |
| 7 | Fe$_3$O$_4$@SiO$_2$/DABCO, H$_2$O, reflux | 25 | 90 | 60 |
| 8 | Fe$_3$O$_4$@MCM-41@Zr-piperazine-MNPs, EtOH/H$_2$O (3 : 7)/reflux | 30 | 85 | 50 |
| 9 | LDH@PTRMS@NDBD@CuI, solvent free, 40 °C | 5 | 96 | This work |

**Table 7** Assessing the effectiveness of the Zn/Cr-LDH@PTRMS@NDBD@CuI catalyst in producing 2-amino-4*H*-chromenes derivatives relative to other catalysts

| Entry | Reaction conditions | Time (min) | Yield (%) | Lit. |
|---|---|---|---|---|
| 1 | PdRu@GO, H$_2$O : EtOH (2 : 1), 80 °C | 12 | 93 | 61 |
| 2 | Fe(HSO$_4$)$_3$, refluxed in MeCN$_2$ | 240 | 83 | 62 |
| 3 | Amino-appended β-cyclodextrin (a3), H$_2$O, r.t | 180 | 94 | 63 |
| 4 | Tungstic acid functionalized mesoporous SBA-15 (TAFMC-1), H$_2$O, reflux | 720 | 80 | 38 |
| 5 | TPOP-2 (40 mg), solvent-free, 80 °C | 240 | 88 | 64 |
| 6 | Sodium carbonate, EtOH/H$_2$O, 25 °C | 84 | 120 | 45 |
| 7 | POPINO, H$_2$O, reflux | 15 | 92 | 43 |
| 8 | Mg/Al: 5.0 hydrotalcite (HT), H$_2$O, 80 °C | 300 | 90 | 46 |
| 9 | LDH@PTRMS@NDBD@CuI, solvent free, 40 °C | 10 | 94 | This work |

featuring various electron-donating and electron-withdrawing substituents, the reactions were performed swiftly, yielding high product yields (Table 5). Benzaldehydes featuring electron-withdrawing groups positioned *ortho* and *para* displayed increased product yields and reduced reaction times. This enhancement can be ascribed to the heightened reactivity of carbonyl benzaldehydes bearing electron-withdrawing groups, which readily react with malononitrile in the catalyst's presence.

The Hammett equation, a fundamental linear free energy equation, delineates the correlation between reaction energetics and the impact of substituents. Changes in the reaction's free energy consequently influence the activation energy of the transition state. Plotting the ratio of rate constants $\log(k_X/k_H)$ against the substituent constant ($\sigma$) for various substituent groups located meta and para to the reaction center, as depicted in Fig. 7 of the Hammett diagram, reveals discernible trends. Notably, the positive slope evident in the Hammett reaction diagram signifies that electron-withdrawing groups augment the reaction rate. However, they lack a substantial impact on the reaction yield.

The proposed mechanism elucidating the synthesis of tetrahydrobenzo[*b*]pyrans and 2-amino-4*H*-chromenes derivatives is depicted in Schemes 2 and 3, respectively, detailing the catalytic pathway. As delineated in Scheme 2, the process initiates with the activation of carbonyl benzaldehyde by the nanocatalyst, rendering it susceptible to nucleophilic attack by activated malononitrile, forming intermediate A. Subsequently,

intermediate A undergoes a reaction with the enolic form of dimedone, yielding intermediate B. With the aid of the catalyst, intermediate B undergoes proton tautomerism to generate intermediate C, followed by intramolecular attack by intermediate C to yield intermediate D. Tautomerization of intermediate D culminates in product formation in the vicinity of the catalyst. Furthermore, the catalyst exhibits recyclability, facilitating its reuse in subsequent cycles.

The proposed mechanism delineating the synthesis of 2-amino-4-*H*-chromenes derivatives is illustrated in Scheme 3. According to this scheme, it becomes evident that intermediate A, activated by the nanocatalyst, primes carbonyl benzaldehyde for nucleophilic attack by malononitrile. This activated state facilitates the reaction between intermediate A and activated resorcinol, leading to the generation of intermediate B. With the catalyst's presence, intermediate B undergoes proton tautomerism, transitioning to intermediate C. Subsequently, intermediate C executes an intramolecular attack, yielding intermediate D. Subsequent tautomerization of intermediate D within the catalyst's vicinity leads to product synthesis, while the catalyst is effectively recycled, reinstated for the next reaction cycle.

To explore the feasibility of recycling and reutilizing the catalyst, a model reaction involving dimedone (1 mmol), 4-chlorobenzaldehyde (1 mmol), and malononitrile (1 mmol) was conducted in the presence of the catalyst. Following the reaction's completion, either ethyl acetate or ethanol was introduced into the reaction mixture, causing the synthesized

product to dissolve in the solvent while the insoluble catalyst was separated *via* centrifugation. Subsequently, the separated catalyst was dried in an oven at 60 °C and utilized in the subsequent reaction. As depicted in Fig. 8, the catalyst was recycled four times without any significant decrease in its efficiency.

In order to demonstrate the effectiveness of the newly developed catalyst, a comparative study was undertaken, evaluating it against alternative catalysts in the synthesis of tetrahydrobenzo[*b*]pyrans and 2-amino-4*H*-chromenes through a three-component reaction. The detailed findings are presented in Tables 6 and 7. The results depicted in these tables underscore the considerable enhancement afforded by the current catalyst in optimizing reaction conditions. Remarkably, with the LDH@PTRMS@NDBD@CuI catalyst, both reaction time and temperature decreased, while product yield increased, underscoring the heightened efficiency of the current catalyst.

# 4. Conclusion

In brief, a novel approach was devised for fabricating the LDH@PTRMS@NDBD@CuI nanocatalyst, integrating copper iodide nanoparticles onto a nanocomposite derived from a modified layered double hydroxide with $N_1,N_4$-bis(4,6-diamino-1,3,5-triazin-2-yl)benzene-1,4-disulfonamide (NDBD). Validation of this catalyst was meticulously conducted using various instrumental techniques, demonstrating its remarkable efficacy and recyclability when deployed in a one-pot three-component reaction for synthesizing tetrahydrobenzo[*b*]pyrans and 2-amino-4*H*-chromenes compounds under soft conditions. Notably, this method champions green chemistry principles by eliminating toxic organic solvents. Some of its main benefits include using easily accessible raw materials, a simplified single-step reaction process, reduced reaction time, simple product purification, eco-friendly, and increase product yield. Furthermore, the catalyst exhibits exceptional reusability, maintaining significant efficiency over up to four cycles with ease of extraction from the reaction mixture. This catalyst holds promise for synthesizing new heterocycles, highlighting its prospective utility in forthcoming endeavors.

# Data availability

The data supporting this article have been included as part of the ESI.†

# Author contributions

R. G. H. and S. M. conceived the experiments and provided experimental instructions, S. M. performed the experiments, analyzed the results and wrote the manuscript. The authors reviewed and revised the manuscript.

# Conflicts of interest

The authors declare no competing interests.

# Acknowledgements

# References

1 S. Mondal, S. Dasgupta and K. Maji, MgAl- Layered Double Hydroxide Nanoparticles for controlled release of Salicylate, *Mater. Sci. Eng. C*, 2016, **68**, 557–564.

2 S. Momeni and R. Ghorbani-Vaghei, Copper Immobilized on Modified LDHs as a Novel Efficient Catalytic System for Three-Component Synthesis of Pyrano[2,3-d]pyrimidine and pyrazolo[4′,3′:5,6]pyrano[2,3-d]pyrimidine Derivatives, *ACS Omega*, 2024, **9**, 10299–10331.

3 F. Tang, H. Bai, Y. Chen, C. Shi, D. Wang, Y. Zhang, W. Liu, L. Yang and L. Hu, CoAl-LDH decorated with cerium oxide as an efficient adsorbent for restoring low-concentration phosphate in wastewater, *RSC Adv.*, 2024, **14**, 10056–10069.

4 S. Khan, S. Khan and A. Asiri, Toward the design of Zn–Al and Zn–Cr LDH wrapped in activated carbon for the solar assisted de-coloration of organic dyes, *RSC Adv.*, 2016, **6**, 83196–83208.

5 Y. Zhang, H. Xu and S. Lu, Preparation and application of layered double hydroxide nanosheets, *RSC Adv.*, 2021, **11**, 24254–24281.

6 S. Momeni and R. Ghorbani-Vaghei, Synthesis, properties, and application of the new nanocatalyst of double layer hydroxides in the one-pot multicomponent synthesis of 2-amino-3-cyanopyridine derivatives, *Sci. Rep.*, 2023, **13**, 1627.

7 M. P. Figueiredo, V. R. R. Cunha, F. Leroux, C. Taviot-Gueho, M. N. Nakamae, Y. R. Kang, R. B. Souza, A. M. C. R. P. F. Martins, I. H. J. Koh and V. R. L. Constantino, Iron-Based Layered Double Hydroxide Implants: Potential Drug Delivery Carriers with Tissue Biointegration Promotion and Blood Microcirculation Preservation, *ACS Omega*, 2018, **3**, 18263–18274.

8 X. He, Z. Jiang, O. U. Akakuru, J. Li and A. Wu, Nanoscale covalent organic frameworks: from controlled synthesis to cancer therapy, *Chem. Commun.*, 2021, **57**, 12417–12435.

9 Z. Jiang, X. Han, C. Zhao, S. Wang and X. Tang, Recent Advance in Biological Responsive Nanomaterials for Biosensing and Molecular Imaging Application, *Int. J. Mol. Sci.*, 2022, **23**, 1923.

10 A. P. Katariya, A. R. Yadav, O. B. Pawar, P. M. Pisal, J. N. Sangshetti, M. V. Katariya and S. U. Deshmukh, An Efficient and Green Synthesis of Tetrahydrobenzo[b]Pyran Derivatives Using [(EMIM)Ac] at Room Temperature, *ChemistrySelect*, 2022, **7**, e202104184.

11 S. Momeni and R. Ghorbani-Vaghei, Green synthesis of quinazoline derivatives using a novel recyclable nanocatalyst of magnetic modified graphene oxide supported with copper, *Sci. Rep.*, 2023, **13**, 1–17.

12 M. M. Khan, S. Khan and S. Iqbal, Recent developments in multicomponent synthesis of structurally diversified tetrahydropyridines, *RSC Adv.*, 2016, **6**, 42045–42061.

13 W. Zuo, L. Zuo, X. Geng, Z. Li and L. Wang, Radical-Polar Crossover Enabled Triple Cleavage of CF2Br2: A Multicomponent Tandem Cyclization to 3-Fluoropyrazoles, *Org. Lett.*, 2023, **25**, 6062–6066.

14 T. Symeonidis, M. Chamilos, D. J. Hadjipavlou-Litina, M. Kallitsakis and K. E. Litinas, Synthesis of hydroxycoumarins and hydroxybenzo[f]- or [h]coumarins as lipid peroxidation inhibitors, *Bioorg. Med. Chem. Lett.*, 2009, **19**, 1139–1142.

15 Z. Zeng, C. Liao and L. Yu, Molecules for COVID-19 treatment, *Chinese Chem. Lett.*, 2024, **35**, 109349.

16 A. Khazaei, F. Gholami, V. Khakyzadeh, A. R. Moosavi-Zare and J. Afsar, Magnetic core–shell titanium dioxide nanoparticles as an efficient catalyst for domino Knoevenagel–Michael-cyclocondensation reaction of malononitrile, various aldehydes and dimedone, *RSC Adv.*, 2015, **5**, 14305–14310.

17 D. Kumar, V. B. Reddy, S. Sharad, U. Dube and S. Kapur, A facile one-pot green synthesis and antibacterial activity of 2-amino-4H-pyrans and 2-amino-5-oxo-5,6,7,8-tetrahydro-4H-chromenes, *Eur. J. Med. Chem.*, 2009, **44**, 3805–3809.

18 X. Yu and X. Hu, Zhou and Zhongqiang, Green and Efficient One-Pot Synthesis of 2-Amino-3-phenylsulphonyl-4H-chromenes under Solvent-Free Conditions, *Iran. J. Chem. Chem. Eng.*, 2018, **37**, 31–38.

19 N. Latif, N. Mishriky and F. M. Assad, Carbonyl and thiocarbonyl compounds. XIX. Intramolecular cyclization of (2-nitroetheny1)aryl N-arylcarbamates : synthesis of newer series of 3,4-dihydro-2H-1,3-oxazin-2-ones and their antimicrobial activities, *Aust. J. Chem.*, 1982, **35**, 1037–1043.

20 L. Bonsignore, G. Loy, D. Secci and A. Calignano, Calignano, Synthesis and pharmacological activity of 2-oxo-(2H) 1-benzopyran-3-carboxamide derivatives, *Eur. J. Med. Chem.*, 1993, **28**, 517–520.

21 A. D. Patil, A. J. Freyer, D. S. Eggleston, R. C. Haltiwanger, M. F. Bean, P. B. Taylor, M. J. Caranfa, A. L. Breen, H. R. Bartus, R. K. Johnson, R. P. Hertzberg and J. W. Westley, The Inophyllums, Novel Inhibitors of HIV-1 Reverse Transcriptase Isolated from the Malaysian Tree, Calophyllum inophyllum Linn, *J. Med. Chem.*, 1993, **36**, 4131–4138.

22 J. B. Chylińska, T. Urbański and M. Mordarski, Dihydro-1,3-oxazine Derivatives and their Antitumor Activity, *J. Med. Chem.*, 1963, **6**, 484–487.

23 P. W. Smith, S. L. Sollis, P. D. Howes, P. C. Cherry, I. D. Starkey, K. N. Cobley, H. Weston, J. Scicinski, A. Merritt, A. Whittington, P. Wyatt, N. Taylor, D. Green, R. Bethell, S. Madar, R. J. Fenton, P. J. Morley, T. Pateman and A. Beresford, Dihydropyrancarboxamides related to zanamivir: a new series of inhibitors of influenza virus sialidases. 1. Discovery, synthesis, biological activity, and structure-activity relationships of 4-guanidino- and 4-amino-4H-pyran-6-carboxamides, *J. Med. Chem.*, 1998, **41**, 787–797.

24 D. O. Moon, K. C. Kim, C. Y. Jin, M. H. Han, C. Park, K. J. Lee, Y. M. Park, Y. H. Choi and G. Y. Kim, Inhibitory effects of eicosapentaenoic acid on lipopolysaccharide-induced activation in BV2 microglia, *Int. Immunopharmacol.*, 2007, **7**, 222–229.

25 S. X. Cai, J. Drewe and W. Kemnitzer, Discovery of 4-aryl-4H-chromenes as potent apoptosis inducers using a cell-and caspase-based Anti-cancer Screening Apoptosis Program (ASAP): SAR studies and the identification of novel vascular disrupting agents, *Anticancer Agents Med. Chem.*, 2009, **9**, 437–456.

26 J. Yang, S. Liu, H. Hu, S. Ren and A. Ying, One-pot three-component synthesis of tetrahydrobenzo[b]pyrans catalyzed by cost-effective ionic liquid in aqueous medium, *Chinese J. Chem. Eng.*, 2015, **23**, 1416–1420.

27 H. Maleki, J. Rakhtshah and B. Shaabani, Effective one-pot synthesis of tetrahydrobenzo[b]pyran derivatives using nickel Schiff-base complex immobilized on iron oxide nanoparticles, *Appl. Organomet. Chem.*, 2020, **34**, e5683.

28 G. Sabitha, K. Arundhathi, K. Sudhakar, B. S. Sastry and J. S. Yadav, Cerium(III) Chloride–Catalyzed One-Pot Synthesis of Tetrahydrobenzo[b]pyrans, *Synth. Commun.*, 2009, **39**, 433–442.

29 A. El Hallaoui, S. Chehab, B. Malek, O. Zimou, T. Ghailane, S. Boukhris, A. Souizi and R. Ghailane, Valorization of the Modified Mono Ammonium Phosphate by Cobalt in the Synthesise of 3,4-Dihydropyrano[c]chromene Derivatives, *ChemistrySelect*, 2019, **4**, 3062–3070.

30 P. Singh, P. Yadav, A. Mishra and S. K. Awasthi, Green and Mechanochemical One-Pot Multicomponent Synthesis of Bioactive 2-amino-4H-benzo[b]pyrans via Highly Efficient Amine-Functionalized SiO2@Fe3O4 Nanoparticles, *ACS Omega*, 2020, **5**, 4223–4232.

31 P. Patil, S. Kadam, D. Patil and P. More, An eco-friendly innovative halide and metal-free basic ionic liquid catalyzed synthesis of tetrahydrobenzo[b]pyran derivatives in aqueous media: A sustainable protocol, *J. Mol. Liq.*, 2022, **345**, 117867.

32 M. Mehravar, B. B. F. Mirjalili, E. Babaei and A. Bamoniri, Nano-SiO2/DBN: an efficacious and reusable catalyst for one-pot synthesis of tetrahydrobenzo[b]pyran derivatives, *BMC Chem.*, 2021, **15**, 34.

33 M. Kidwai, S. Saxena, M. K. R. Khan and S. S. Thukral, Aqua mediated synthesis of substituted 2-amino-4H-chromenes and in vitro study as antibacterial agents, *Bioorg. Med. Chem. Lett.*, 2005, **15**, 4295–4298.

34 M. M. Khafagy, A. H. F. Abd El-Wahab, F. A. Eid and A. M. El-Agrody, Synthesis of halogen derivatives of benzo[h]chromene and benzo[a]anthracene with promising antimicrobial activities, *Farm*, 2002, **57**, 715–722.

35 K. Hiramoto, A. Nasuhara, K. Michikoshi, T. Kato and K. Kikugawa, DNA strand-breaking activity and mutagenicity of 2,3-dihydro-3,5-dihydroxy-6-methyl-4H-pyran-4-one (DDMP), a Maillard reaction product of glucose and glycine, *Mutat. Res. Toxicol. Environ. Mutagen.*, 1997, **395**, 47–56.

36 L. Alvey, S. Prado, B. Saint-Joanis, S. Michel, M. Koch, S. T. Cole, F. Tillequin and Y. L. Janin, Diversity-oriented synthesis of furo[3,2-f]chromanes with antimycobacterial activity, *Eur. J. Med. Chem.*, 2009, **44**, 2497–2505.

37 A. M. Fouda, Synthesis of several 4H-chromene derivatives of expected antitumor activity, *Med. Chem. Res.*, 2016, **25**, 1229–1238.

38 S. K. Kundu, J. Mondal and A. Bhaumik, Tungstic acid functionalized mesoporous SBA-15: a novel heterogeneous catalyst for facile one-pot synthesis of 2-amino-4H-chromenes in aqueous medium, *Dalton Trans.*, 2013, **42**, 10515–10524.

39 J. Safari and L. Javadian, Ultrasound assisted the green synthesis of 2-amino-4H-chromene derivatives catalyzed by Fe3O4-functionalized nanoparticles with chitosan as a novel and reusable magnetic catalyst, *Ultrason. Sonochem.*, 2015, **22**, 341–348.

40 J. Albadi, A. Razeghi, A. Mansournezhad and Z. Azarian, CuO-CeO2 nanocomposite catalyzed efficient synthesis of aminochromenes, *J. Nanostructure Chem.*, 2013, **3**, 1–5.

41 D. Kumar, V. B. Reddy, B. G. Mishra, R. K. Rana, M. N. Nadagouda and R. S. Varma, Nanosized magnesium oxide as catalyst for the rapid and green synthesis of substituted 2-amino-2-chromenes, *Tetrahedron*, 2007, **63**, 3093–3097.

42 M. Saikia and L. Saikia, Sulfonic acid-functionalized MIL-101(Cr) as a highly efficient heterogeneous catalyst for one-pot synthesis of 2-amino-4H-chromenes in aqueous medium, *RSC Adv.*, 2016, **6**, 15846–15853.

43 M. Dekamin, M. Eslami and A. Maleki, Potassium phthalimide-N-oxyl: a novel, efficient, and simple organocatalyst for the one-pot three-component synthesis of various 2-amino-4H-chromene derivatives in water, *Tetrahedron*, 2013, **69**, 1074–1085.

44 M. Kidwai and R. Poddar, Transesterification of chromenes employing immobilized lipase in ionic liquids, *Catal. Lett.*, 2008, **124**, 311–317.

45 N. Dinh Thanh, D. Son Hai, V. Thi Ngoc Bich, P. Thi Thu Hien, N. Thi Ky Duyen, N. Thi Mai, T. Thi Dung, H. Thi Kim Van, V. Ngoc Toan, N. H. Huy, T. Thi Thanh Van, D. Ngoc Toan and L. Hai Dang, Synthesis and structure of some substituted 2-amino-4-aryl-7-propargyloxy-4H-chromene-3-carbonitriles, *Synth. Commun.*, 2019, **49**, 102–117.

46 S. R. Kale, S. S. Kahandal, A. S. Burange, M. B. Gawande and R. V Jayaram, A benign synthesis of 2-amino-4H-chromene in aqueous medium using hydrotalcite (HT) as a heterogeneous base catalyst, *Catal. Sci. Technol.*, 2013, **3**, 2050–2056.

47 Z. Karamshahi, R. Ghorbani-Vaghei and N. Sarmast, Efficient synthesis of multiply substituted 7H-indeno [2, 1-c] quinoline using 7-aminonaphthalene-1, 3-disulfonic acid supported on LDHs as catalyst, *Mater. Sci. Eng. C*, 2019, **9**, 45–54.

48 J. Zhu, H. Fan, J. Sun and S. Ai, Anion-exchange precipitation synthesis of α-Ag2WO4/Zn–Cr layered double hydroxides composite with enhanced visible-light-driven photocatalytic activity, *Sep. Purif. Technol.*, 2013, **120**, 134–140.

49 S. Rohani and A. Ziarati, CuI Nanoparticles as a Reusable Heterogeneous Catalyst for the One-Pot Synthesis of N-Cyclohexyl-3-aryl-quinoxaline-2-amines Under Mild Conditions, *J Nanostruct.*, 2012, **2**, 79–83.

50 R. Pourhasan-Kisomi, F. Shirini and M. Golshekan, Introduction of organic/inorganic Fe3O4@MCM-41@Zr-piperazine magnetite nanocatalyst for the promotion of the synthesis of tetrahydro-4H-chromene and pyrano[2,3-d] pyrimidinone derivatives, *Appl. Organomet. Chem.*, 2018, **32**, e4371.

51 H. Faroughi Niya, N. Hazeri, M. Rezaie Kahkhaie and M. T. Maghsoodlou, Preparation and characterization of MNPs–PhSO₃H as a heterogeneous catalyst for the synthesis of benzo[b]pyran and pyrano[3,2-c]chromenes, *Res. Chem. Intermed.*, 2020, **46**, 1685–1704.

52 P. Mohammadi and H. Sheibani, Synthesis and characterization of Fe₃O₄@SiO₂ guanidine-poly acrylic acid nanocatalyst and using it for one-pot synthesis of 4H-benzo [b] pyrans and dihydropyrano [c] chromenes in water, *Mater. Chem. Phys.*, 2019, **22**, 140–146.

53 O. H. Qareaghaj, S. Mashkouri, M. R. Naimi-Jamal and G. Kaupp, Ball milling for the quantitative and specific solvent-free Knoevenagel condensation + Michael addition cascade in the synthesis of various 2-amino-4-aryl-3-cyano-4 H -chromenes without heating, *RSC Adv.*, 2014, **4**, 48191–48201.

54 S. Pan, P. Li, G. Xu, J. Guo, L. Ke, C. Xie, Z. Zhang and Y. Hui, MCM-41@Schiff base-Co(OAc)2 as an efficient catalyst for the synthesis of pyran derivatives, *Res. Chem. Intermed.*, 2020, **46**, 1353–1371.

55 M. Bayzidi and B. Zeynizadeh, The Immobilized Zirconocene Chloride on Magnetite-reduced Graphene Oxide: A Highly Efficient and Reusable Heterogeneous Nanocatalyst for One-pot Three-component Synthesis of Tetrahydrobenzo[b] pyrans and Dihydropyrano[3,2-c]chromenes, *ChemistrySelect*, 2022, **7**, e202202708.

56 D. Azarifar and M. Khaleghi-Abbasabadi, Fe₃O₄-supported N-pyridin-4-amine-grafted graphene oxide as efficient and magnetically separable novel nanocatalyst for green synthesis of 4H-chromenes and dihydropyrano[2,3-c] pyrazole derivatives in water, *Res. Chem. Intermed.*, 2019, **45**, 199–222.

57 A. A. Mohammadi, M. R. Asghariganjeh and A. Hadadzahmatkesh, Synthesis of tetrahydrobenzo[b] pyran under catalysis of NH₄Al(SO₄)₂·12H₂O (Alum), *Arab. J. Chem.*, 2017, **10**, S2213–S2216.

58 B. Maleki, H. Eshghi, M. Barghamadi, N. Nasiri, A. Khojastehnezhad, S. Sedigh Ashrafi and O. Pourshiani, Silica-coated magnetic NiFe₂O₄ nanoparticles-supported H₃PW₁₂O₄₀; Synthesis, preparation, and application as an efficient, magnetic, green catalyst for one-pot synthesis of tetrahydrobenzo[b]pyran and pyrano[2,3-c]pyrazole derivatives, *Res. Chem. Intermed.*, 2016, **42**, 3071–3093.

59 H. Kiyani and F. Ghorbani, Potassium phthalimide promoted green multicomponent tandem synthesis of 2-amino-4H-chromenes and 6-amino-4H-pyran-3-carboxylates, *J. Saudi Chem. Soc.*, 2014, **18**, 689–701.

60 J. Davarpanah, A. Kiasat, S. Noorizadeh and M. Ghahremani, Nano magnetic double-charged diazoniabicyclo [2.2. 2]

octane dichloride silica hybrid: synthesis, characterization, and application as an efficient and reusable organic–inorganic hybrid silica with ionic liquid framework for one-pot synthesis of pyran annulated heterocyclic compounds in water, *J. Mol. Catal. A Chem.*, 2013, **376**, 78–89.

61 B. Şen, N. Lolak, Ö. Paralı, M. Koca, A. Şavk, S. Akocak and F. Şen, Bimetallic PdRu/graphene oxide based catalysts for one-pot three-component synthesis of 2-amino-4H-chromene derivatives, *Nano-Structures Nano-Objects*, 2017, **12**, 33–40.

62 H. Eshghi, S. Damavandi and G. H. Zohuri, Efficient One-Pot Synthesis of 2-Amino-4H-chromenes Catalyzed by Ferric Hydrogen Sulfate and Zr-Based Catalysts of FI, *Synth. React. Inorg. Met. Org. Chem.*, 2011, **41**, 1067–1073.

63 Y. Ren, B. Yang and X. Liao, The amino side chains do matter: chemoselectivity in the one-pot three-component synthesis of 2-amino-4H-chromenes by supramolecular catalysis with amino-appended β-cyclodextrins (ACDs) in water, *Catal. Sci. Technol.*, 2016, **6**, 4283–4293.

64 S. K. Kundu and A. Bhaumik, A triazine-based porous organic polymer: a novel heterogeneous basic organocatalyst for facile one-pot synthesis of 2-amino-4H-chromenes, *RSC Adv.*, 2015, **5**, 32730–32739.